Proceedings of the Thirty-second (2022) International Ocean and Polar Engineering Conference **www.isope.org**
Shanghai, China, June 5–10, 2022

ISBN 978-1-880653-81-4; ISSN 1098-6189

Research on the Tip Vortex Cavitation and Its Control of an Elliptical Hydrofoil

Kang Liu[1], Jianwei Wu[2], Liushuai Cao[1], Decheng Wan[1]*

[1] Computational Marine Hydrodynamics Lab (CMHL), School of Naval Architecture, Ocean and Civil Engineering,
Shanghai Jiao Tong University, Shanghai, China
[2] Wuhan Second Ship Design and Research Institute, Wuhan, China
[*]Corresponding author

ABSTRACT

The tip vortex induced cavitation affects the performance of the thrusters and causes noise radiation and vibration. Thus, it is desirable to know how to predict and control the tip vortex cavitation (TVC) and understand its mechanism, which a full understanding has not yet been achieved. In this work, we perform TVC simulation of wetted and cavitating flows around an elliptical hydrofoil with the cross section of NACA0012 and try to control the cavitation inception by injecting water. In order to capture the TVC induced by the hydrofoil, adaptive mesh refinement (AMR) method is used for the mesh refinement in the wake region, especially the tip vortex region. Two steps are undertaken, firstly, to reveal the characteristics of the tip vortex and TVC, the simulations are performed under the wetted flow and cavitating flow, respectively. After that, we introduce the water injection method to reduce and suppress the cavitation inception. The improved delayed Detached Eddy Simulation (IDDES) turbulence modeling method and Schnerr-Sauer cavitation model are applied to guarantee the accuracy and speed of the prediction. The lift coefficients in this paper agree fairly well with the experimental data and the max error is 5.5%, which is acceptable in engineering field. Results show that the strong swirling flow of the tip vortex region is the main reason of TVC inception. Furthermore, the presence of TVC will increase the dilatation and baroclinic torque component of the tip vortex. And the injection of water has an obvious suppression effect on the TVC inception.

KEY WORDS: elliptical hydrofoil; tip vortex cavitation; water injection; adaptive mesh refinement; IDDES

INTRODUCTION

Cavitation is the cyclic process of the formation, development and collapse of cavitation bubbles during the vapor-liquid transformation. For offshore machinery, it is a commonly occurring phenomenon. During its working process, velocity acceleration is accompanied with pressure reduction, and so that the liquid will transit to the gaseous phase. There are different types of cavitation according to the structures of cavitation bubble (sheet, cloud, tip vortex cavitation, etc.). Among them, tip vortex cavitation (TVC) is a common type in marine rotating machineries. For example, propeller or elliptical hydrofoil generates tip vortex cavitation when working at a high speed.

Different with the sheet cavitation on the surface of propeller or foil, tip vortex cavitation only slightly affects the hydrodynamic performance and efficiency of power machineries (Liu. 2019). However, during the development of the tip vortex, the collapse of the cavitation bubble produces a pressure pulsation and lead to greatly increasing of the working noise. The noise will reduce the comfort of the ship, and even more, for military ships and submarine, the noise will expose them to the enemy's detection sonar, greatly reducing the concealment and safety of the warships. In addition, when the flow develops backward to the ambient region of the rudder, TVC also affects the usage of the rudder and reduce its efficiency. And the attachment of the TVC bubble on the rudder surface leads to the erosion of the rudder surface and reduce its working life (Chen. 2019). Therefore, it is necessary to know the mechanism of TVC and how to forecast and control it.

In the research of tip vortex cavitation, scholars have done some works. Ji et al. (2014) have studied the interaction between cavitation and vortex with Delft Twist-11 hydrofoil. After analyzing the proportions of each component in the vorticity transport equation around tip vortex region, it is found that the dilatation term increases significantly when cavitation occurs, and its amplitude reaches the same level as the vortex stretching term. At the same time, Cheng et al. (2020) simulated the tip leakage vortex of the NACA0009 hydraulic hydrofoil by Large Eddy Simulation (LES) method and obtained the same result.

Xie et al. (2021) have numerically studied the tip vortex flow around NACA16-020 elliptical hydrofoil. Based on the interaction of cavitation, vortex, and turbulence analyzation, it is clearly shown that the cavitation promotes the production of vorticity and increases the thickness of boundary layer. To explore the effect of TVC on tip vortex, Ohta et al. (2019) simulates cavitation at the turbulent boundary layer near the wall under the condition of Re=2000-2600. The results show that when cavitation occurs, cavitation will impede the exchange of turbulent kinetic energy, and reduce the momentum transfer from the vortex core to other directions.

In recent years, the inhibitory effect of mass injection methods on cavitation is a hot issue. Chang et al. (2011) finds that by injecting water or water-based polymer into the core zone of the tip vortex, TVC generation can be effectively inhibited, and water injection reduces the flow instability in the vortex core area. Timoshevskiy et al. (2016)

studies the effect of tangential injection on the suction surface of the hydrofoil. The results show that tangential injection can effectively reduce the area of cloud cavitation and achieve effective suppression for cavitation. Lee et al. (2018) applies water injection on elliptical hydrofoils and propellers. In the analyzation of Lee, mass injection can successfully inhibit TVC and reduce TVC noise level, and the higher the injection velocity, the more obvious suppression for tip vortex cavitation.

According to the existing research, it is clear that the active injection control can effectively inhibit the cavitation of the hydrofoil and propeller. At the same time, water injection near the tip region can effectively suppress the operating noise generation. However, the research on the mechanism of TVC generation and mass injection for cavitation control are still unclear, and there are relatively few studies on the interaction between water jet, tip vortex and tip vortex cavitation.

In this paper, STAR-CCM+ software is used to simulate the tip vortex cavitation phenomenon of an elliptical hydrofoil with the cross section of NACA0012, which is based on the IDDES turbulence model and Schnerr-Sauer cavitation model. Furthermore, water injection method is used to control the cavitation inception. In the simulation, firstly, the hydrodynamic performance of the hydrofoil is calculated for numerical validation; secondly, to reveal the characteristics of the tip vortex and TVC, the simulation is performed under the wetted flow and cavitating flow, respectively. After that, we introduce the water injection method into cavitation flow condition to suppress the cavitation inception.

NUMERICAL METHODS

Governing Equation

The simulations in hydrodynamic region are based on the Navier-Stokes equations, which mathematically express conservation of momentum and conservation of mass for Newtonian fluids.

$$\frac{\partial \rho}{\partial t}+\frac{\partial(\rho \bar{u}_j)}{\partial x_j}=0 \tag{1}$$

$$\frac{\partial(\rho \bar{u}_j)}{\partial t}+\frac{\partial(\rho \bar{u}_i \bar{u}_j)}{\partial x_j}=-\frac{\partial p}{\partial x_j}+\frac{\partial}{\partial x_j}\left((\mu+\mu_t)(\frac{\partial u_i}{\partial x_j}+\frac{\partial u_j}{\partial x_i})\right) \tag{2}$$

In the above equation, $\bar{u}_j$ is the time average velocity; u_j' is the pulsating velocity; μ_t is the turbulent viscosity coefficient; ρ is the density; and μ is the viscosity coefficient under single-phase homogenization.

Turbulence Modelling

When solving the engineering problems, scholars have simplified the N-S equations by different theoretical assumptions, and three numerical methods have been derived from it, which are Direct Numerical Simulation (DNS), Large Eddy Simulation (LES) and Reynolds-Average Navier-Stokes (RANS).

These methods have their own advantages and weaknesses. DNS and LES method can obtain more accurate calculation result, but require higher mesh quality and longer calculation time. For RANS method, as it only obtains the flow field information in the average sense, less resources are occupied and the results are not accurate enough during simulation.

The Improved Delayed Detached Eddy Simulation (IDDES) method used in this article combines the advantages of LES and RANS. This method is based on the DDES model and redefines the length scale of SubGrid-Scale (SGS) model in LES, so that RANS method can be used when solving the flowing information in the boundary layer region near the wall, and LES method is used in another region. By doing this, IDDES method can obtain more accurate results with less calculation time. Chen et al. (2022) and Wang et al. (2019) used this method to study the performance and wake dynamics of the wind turbines and the effect of bogie fairings, respectively. The governing equation is shown as follows:

$$\frac{\partial \rho k}{\partial t}+\nabla\cdot(\rho \vec{U} k)=\nabla\cdot\left[(\mu+\sigma_k \mu_t)\nabla k\right]+P_k-\rho\sqrt{k^3}/l_{IDDES} \tag{3}$$

$$\frac{\partial \rho \omega}{\partial t}+\nabla\cdot(\rho \vec{U} \omega)=\nabla\cdot\left[(\mu+\sigma_\omega \mu_t)\nabla \omega\right]+2(1-F_1)\rho\sigma_{\omega 2}\frac{\nabla k\cdot\nabla\omega}{\omega}+\alpha\frac{\rho}{\mu_t}P_k-\beta\rho\omega^2 \tag{4}$$

$$\mu_t=\rho\frac{a_1\cdot k}{max(a_1\cdot\omega, F_2\cdot S)} \tag{5}$$

In Eq.3-5, ρ is the density of the fluid, $\vec{U}$ is the velocity, k is the turbulent kinetic energy, ω is the special dissipation of turbulence, S is the magnitude of the strain rate tensor, $\sigma_{\omega 2}$, α, β are the constants. The term F_1, F_2, P_k can be solved by Eq.6-8, and the length scale l_{IDDES} in IDDES reads as Eq.12-15:

$$F_1=tanh(arg_1^4) \tag{6}$$

$$F_2=tanh(arg_2^2) \tag{7}$$

$$P_k=min(\mu_t S^2, 10\cdot C_\mu \rho k\omega) \tag{8}$$

$$CD_{k\omega}=max(2\rho\sigma_{\omega 2}\frac{\nabla k\cdot\nabla\omega}{\omega}, 10^{-10}) \tag{9}$$

$$arg_1=min(max(\frac{\sqrt{k}}{C_\mu\omega d_\omega}, \frac{500v}{d_\omega^2\omega})), \frac{4\rho\sigma_{\omega 2}k}{CD_{k\omega}d_\omega^2} \tag{10}$$

$$arg_2=max(\frac{2\sqrt{k}}{C_\mu\omega d_\omega}, \frac{500v}{d_\omega^2\omega}) \tag{11}$$

Here, d_ω is the distance to the nearest wall, the model constants $C_\mu=0.09$, $\sigma_{\omega 2}=0.856$.

$$l_{IDDES}=\tilde{f}_d\cdot l_{RANS}+(1-\tilde{f}_d)\cdot l_{LES} \tag{12}$$

$$l_{LES}=C_{DES}\Delta \tag{13}$$

$$l_{RANS}=\frac{\sqrt{k}}{C_\mu\omega} \tag{14}$$

$$C_{DES}=C_{DES1}\cdot F_1+C_{DES2}\cdot(1-F_1) \tag{15}$$

Among them, the term Δ, $\tilde{f}_d$ are shown as follow:

$$\Delta=min\{C_\omega max[d_\omega, h_{max}], h_{max}\} \tag{16}$$

$$\tilde{f}_d=max\{(1-f_{dt}), f_b\} \tag{17}$$

$$f_{dt}=1-tanh[(C_{dt1}\cdot r_{dt})^{C_{dt2}}] \tag{18}$$

$$r_{dt}=\frac{\nu_t}{\kappa^2 d_\omega^2\sqrt{0.5(S^2+\Omega^2)}} \tag{19}$$

$$f_b=min\{2exp(-9\alpha^2), 1.0\} \tag{20}$$

$$\alpha=0.25-d_\omega/h_{max} \tag{21}$$

The constants in the models are as follows:

$$C_{\omega} = 0.15, C_{dt1} = 20, C_{dt2} = 3, C_t = 1.87, C_l = 5.0$$

Cavitation Model

Cavitation models can be divided into two categories: the first is the model based on the state equation, and the other is based on the transport equation.

As the evaporation and condensation process of the liquid can be simulated, the real cavitation details can be more authentic in the cavitation models through the transportation equation. The transport equation is as follows:

$$\frac{\partial \alpha_v \rho_v}{\partial t} + \frac{\partial (\alpha_v \rho_v u_i)}{\partial x_i} = \dot{m}_c + \dot{m}_v \tag{22}$$

Among them, ρ_v is the density of the gas, α_v is the volume fraction of the gas phase, and $\dot{m}_c$ and $\dot{m}_v$ represent the mass expressions in the condensation and vaporization mass exchange processes respectively.

The Schnerr-Sauer cavitation model is one model based on the transport equation. This model has been built into most commercial solvers and widely used in cavitation simulation. For example, Yilmaz et al (2019) simulates propeller TVC based on Schnerr-Sauer cavitation model and Park et al (2021) uses this method to study tip vortex cavitation inception on a foil. In the Schnerr-Sauer cavitation model, $\dot{m}_c$ and $\dot{m}_v$ can be expressed as follows:

$$\dot{m}_c = C_c \frac{3\rho_v \rho_l \alpha_v (1-\alpha_v)}{\rho R} sgn(P_v - P) \sqrt{\frac{2|P_v - P|}{3\rho_l}} \tag{23}$$

$$\dot{m}_v = C_v \frac{3\rho_v \rho_l \alpha_v (1-\alpha_v)}{\rho R} sgn(P_v - P) \sqrt{\frac{2|P_v - P|}{3\rho_l}} \tag{24}$$

where n is the number of voids occupied in the liquid phase, and R is the average void radius.

$$R = \left(\frac{\alpha_v}{1-\alpha_v} \cdot \frac{3}{4\pi n_0}\right)^{1/3} \tag{25}$$

SOLVERS SETUP

Geometric Model and Simulation Setup

As the experiment results of hydrodynamic performance and cavitation can be obtained, the elliptic hydrofoil with NACA0012 section with 150mm maximum chord and 176.7mm span was selected for the tip vortex cavitation simulation in this article, and its geometric model are shown in Fig. 1.

In this study, CFD software STAR-CCM+ is selected for the numerical research, and the trimmed meshing method is adopted for grid meshing. The maximum chord of NACA0012 elliptical hydrofoil is denoted as C, and the axial direction, normal direction and spanwise are denoted as x, y and z. The distance from the inlet to outlet boundary is $16C$, the width and height of this region both are $3C$. NACA0012 elliptical hydrofoil is arranged at the center. The final computational domain is shown in Fig. 2.

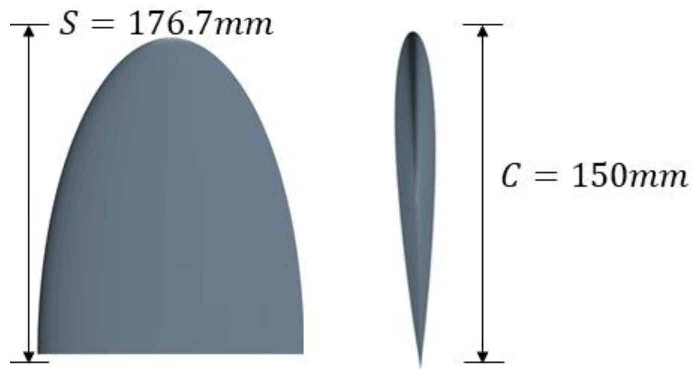

Fig. 1 NACA0012 Elliptic Hydrofoil.

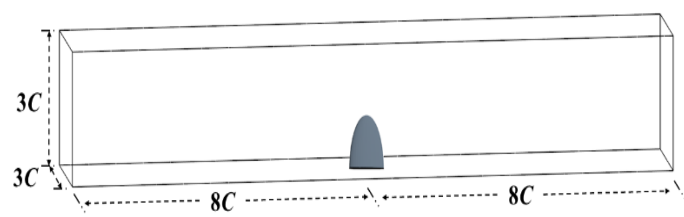

Fig. 2 The numerical domain.

Grid Generation

During vortex roll-up and transport, the tip vortex structures, especially tip vortex cavitation structures of elliptical hydrofoil have very small scales. The flow in vortex core region changes drastically, and a small amount of numerical deviation can cause incorrected results. Thus, grid refinement should be progressed at the tip position before simulation. And as tip vortex is curved along the streamwise and its shape is not a prefect cylinder, it is complicated to refine the position near tip vortex cavitation region by structured meshing method. In this work, the automated meshing tool and volumetric control method by geometry part in STAR-CCM+ is used for grid generating and capture of TVC.

The basic meshing size of domain is set as 0.1C; the maximum cell size in the whole region is set as $0.4C$(approximately equal to 0.06 *mm*); and a smaller grid size ($0.01C$) is used on the hydrofoil surface. To determine the grid refinement resolution, a $8C \times 2C \times 2C$ ($x \times y \times z$) buffer block whose cell size is set as $0.25C$, is used for meshing the region around elliptical hydrofoil. Then, the simulation is undertaken to find the flow trend of tip vortex, so that the first refinement zone can be fixed according the simulation result. Repeat the process and get three cylindrical and one irregular geometry refinement region. These four refinement regions have $0.02C$ for outer cylinder, $0.01C$ for middle cylinder, $0.005C$ for inner cylinder and $0.001C$ for irregular geometry. Fig. 3 shows the location of the refinement regions and the final grid of the domain.

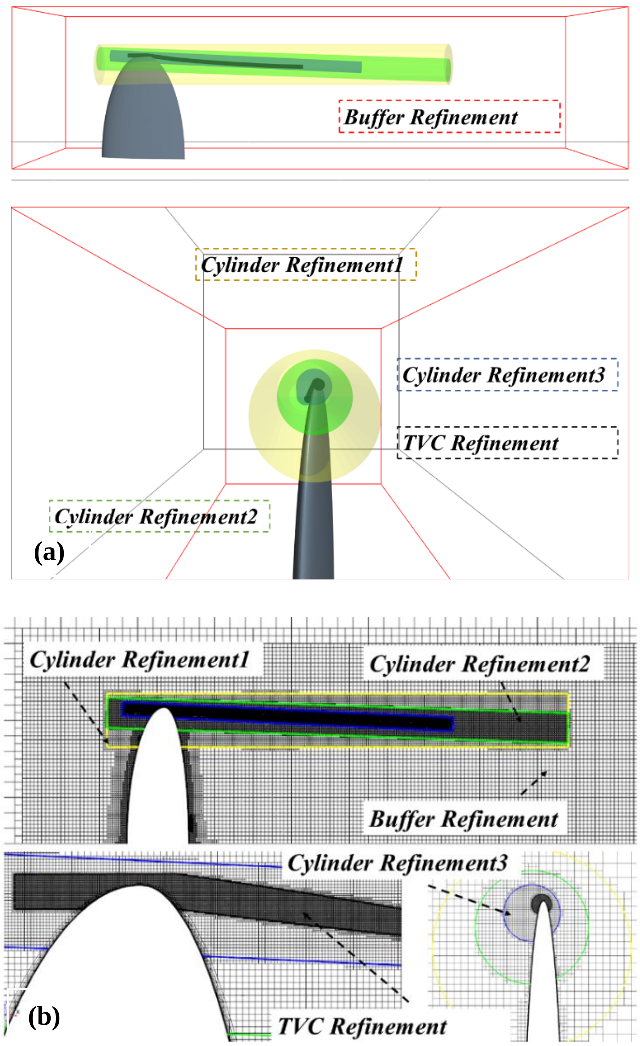

Fig. 3 The location of the refinement regions (a) and the final grid (b).

Boundary Setting and Discretization Format

For the better simulation of the environment of the experimental funnel, the inlet type of the domain is selected as the velocity; the outlet boundary at the downstream is the static pressure outlet; the other boundaries of the far field and hydrofoil surface are set as wall type. The time step $\Delta t = 0.0001s$, and temporal discretization in implicit solver is set as 2$^{\text{nd}}$-order.

NUMERICAL VALIDATION

To verify the accuracy of simulation, the effect of IDDES model has been investigated by lift coefficient C_L of NACA0012 hydrofoil, and the result has been compared to the previous experiment of Takasugi et al (1992).

As shown in Fig. 4, although the error between IDDES and experiment increased as the attack angle increased, the max error rate is about 5.5% and the error rate shown in Table 1 in the condition $\alpha = 10$, which was used in the cavitation simulation following, is about 3.3%. It can be said that lift coefficient in simulation has a good agreement with experiment result, and the accuracy of IDDES model is acceptable in engineering field.

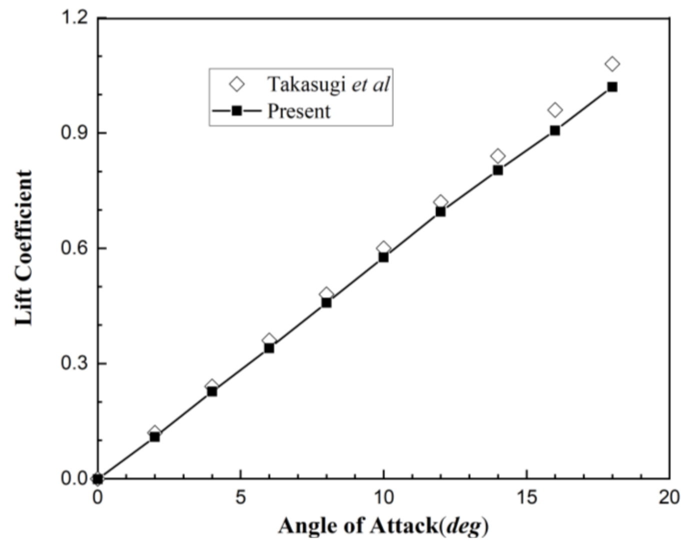

Fig. 4 Lift coefficient comparison between present and experiment.

Table 1. Lift coefficient comparison in cavitation simulation condition.

α	Lift coefficient		Error
	Present	Takasugi et al	
10	0.581	0.60	0.019

Based on tip vortex simulation, the Schnerr-Sauer cavitation model is added in this simulation in this section to explore the mechanism of TVC generation and the interaction between tip vortex and its cavitation. The cavitation in numerical and experiment result are shown in Fig. 5.

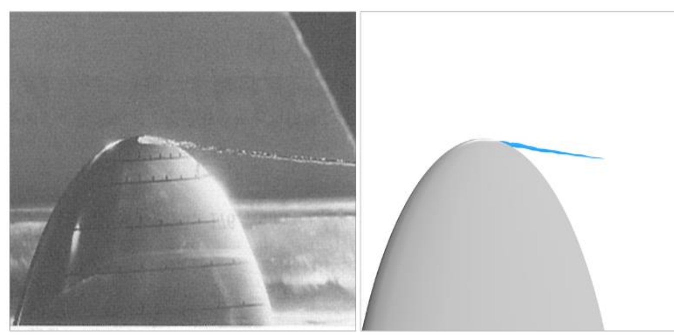

Fig. 5 Cavitation comparison between the results in present and Takasugi et al (1992)

RESULT AND DISCUSSION

Tip Vortex

Before the TVC simulation, the tip vortex flow without cavitation condition has been simulated in this section to get the flow trend around the elliptical hydrofoil and acknowledged the reason of TVC generation. The environment settings of this simulation are shown in Table 2.

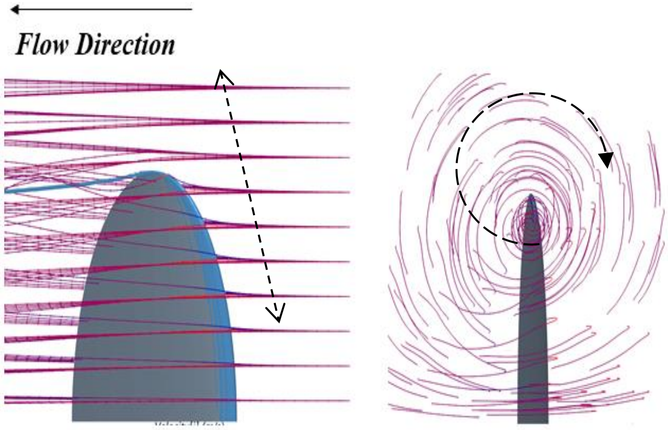

Fig. 6 The flow streamline around NACA0012 hydrofoil.

For figuring out the generation reasons of tip vortex, the flow around the whole region is visualized by the streamline in Fig. 6. And it is clearly illustrated that under the effect of the hydrofoil, the flow around the foil separates into two directions, one part of fluid in the pressure side towards to moving upward while the other tends to move to the suction side and the root of the hydrofoil. Fig. 6 also shows that not just the flow in vortex core region has the rotation action, elliptical hydrofoil affects a wide range of the region having the rotating trend and tip vortex region has the strongest swirling motion.

Table 2. Model settings for NACA0012

Variables	Symbols	Case setting
Inlet velocity	V_I	6.0
Attack angle	α	10
Cavitation number	σ_n	2.01
Vapor Pressure	P_V	3170.34

In the next step, the instantaneous pressure field and cell velocity streamlines on the hydrofoil surface are illustrated in Fig. 7. Fig. 7(a) shows the pressure distribution and flow direction of the pressure side, while the pressure field and streamlines of suction side are displayed in Fig. 7(b).

With the influence of the geometric shape of the elliptical hydrofoil, we can find that the pressure isolines on the surface is not straight along the spanwise, but has the trend bending to the tip. Furthermore, when focusing on the tip region of the foil, it can be shown that the flow trend on the suction side is not simply to flow to the root of the hydrofoil (like shown in Fig. 6). Near the wingtip position, the suction side flow separates into two paths along span direction: one part of the fluid flows to the root of the foil, while the other shows an upward movement trend. Therefore, the fluid confluence position is not at the foil tip-position, but the leading edge close to the tip, that is, the tip vortex is initially generated at the leading edge. According to the density of streamlines in Fig. 7, it is clear that the flow velocity near the tip region is higher that another region. Thus, the tip vortex intensity generated after the confluence is stronger than others region.

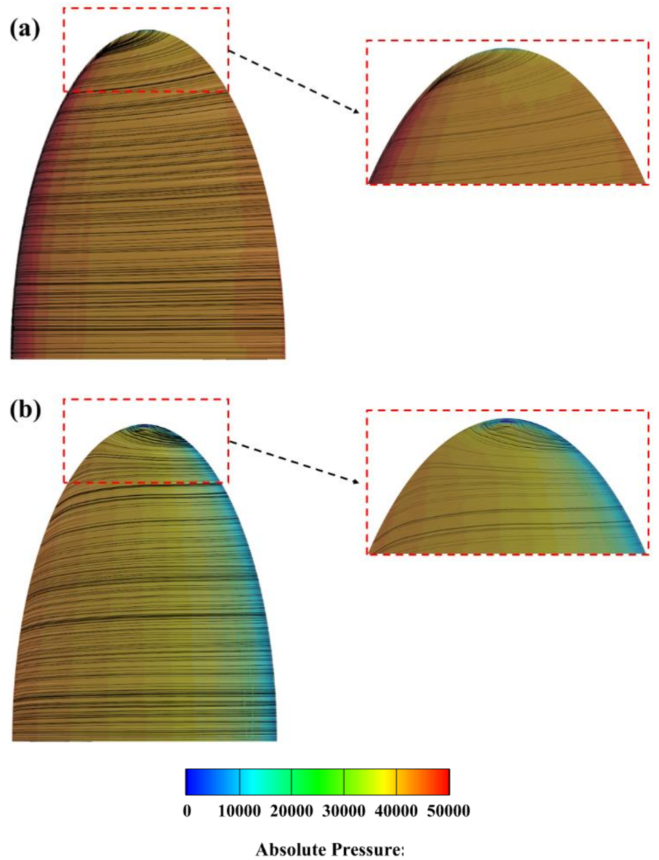

Fig. 7 The pressure distribution and cell velocity streamline of the NACA0012 elliptical hydrofoil: (a) pressure side; (b) suction side.

TVC Simulation

In the next step, TVC of NACA0012 elliptical hydrofoil should be simulated. However, due to the flow structure scalers of TVC is smaller than tip vortex, the grid size in this paper is suitable for the capture of tip vortex but not enough to simulate TVC. Therefore, the adaptive refinement method is introduced. STAR-CCM+ has available adaptive mesh tool, and users only need to customize the refinement criterion.

As the cavitation occurs during tip vortices developing, and the tip vortices flow always contains cavitation bubbles. When defining the adaptive criterion, the absolute pressure field function is used. If the absolute pressure is between 3170Pa and 8000Pa, the grid will be refined, or the grid will remain the same. In this way, the areas where vortex cavitation likely to occur will be refined, and the areas where the cavitation has occurred will not be over refined.

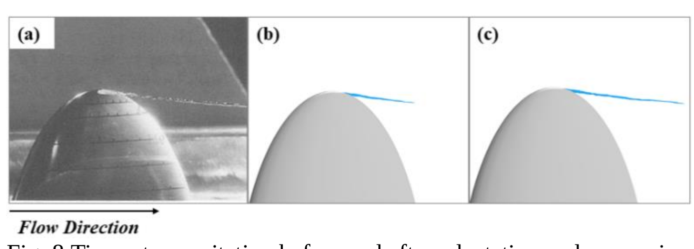

Fig. 8 Tip vortex cavitation before and after adaptation and comparison with EFD: (a) EFD tip vortex cavitation in Takasugi et al (1992); (b) tip vortex cavitation before adaptation; (c) tip vortex cavitation after adaptation.

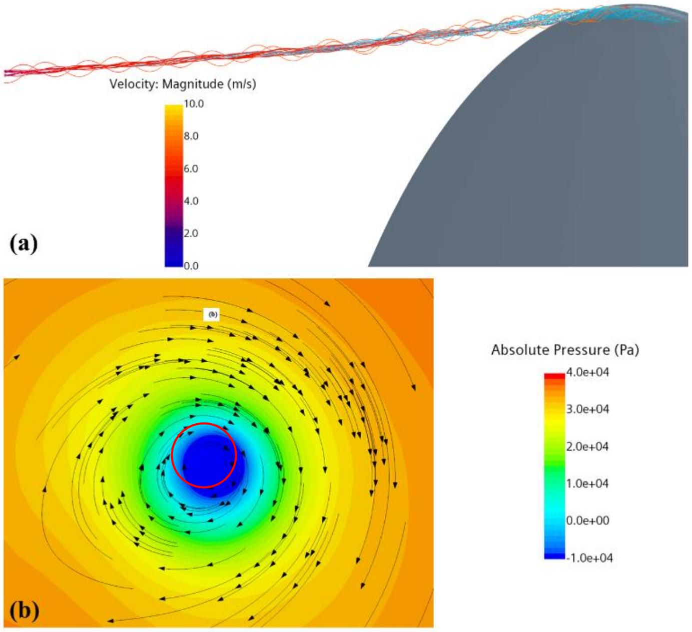

Fig. 9 Streamline near the cavitation region and pressure cloud of TV at $x = 0.2C$

The vapor structure of TVC in simulation is visualized by isosurface of $\alpha_v = 0.1$, while $\alpha_v$is denoted as the volume fraction of water vapor. Fig. 8 shows the cavitation development before and after adaptation and comparison with the experiment result of Takasugi et al (1992). It can be found that TVC isosurface after meshing adaptation is longer than it before AMR, and adaptive meshing method has significantly increased the development of the tip vortex cavitation. The final vapor volume grows to $3.8 \times 10^{-7} m^3$ from $3.2 \times 10^{-7} m^3$. Grow rate is 18.7%. And total grid increases to 12 million.

To acknowledge the cause reason of the tip vortex cavitation, the plot of the flow trend at the tip vortex cavitation position has been illustrated, as shown in the Fig. 9(a). It can be seen that the flow around the tip vortex is in a spiral shape, and after observing the pressure distribution on the slice at $x = 0.2C$ in Fig. 9(b), the cloud shows that there is a very obvious pressure reduction at the tip vortex core zone. Apparently, this phenomenon is mainly caused by the rotational movement in the y-z plane, called swirling effect of the tip vortex.

Next, we analyzed the reaction of TVC to the tip vortex, and the Q' cloud diagram on the $x = 0.2C$ slide has been performed in the Fig. 10. In this Figure, (a) is the structure of tip vortex in wetted flow, and (b) is the structure under cavitation condition. Q' denote as the non-dimensionalized parameter of Q-criterion by U^2/C^2.

Comparing the differences between these two figures, we can find that: on the one hand, when tip vortex cavitation occurs, vortex motion inside the cavity is basically zero, as shown in the area marked in red color in Fig. 10(b). On the other hand, cavitation increases the diameter of the vortex core region and slightly change the shape of the tip vortex core. The shape of the vortex core is a perfect circle under the wetted flow condition, while the shape of the vortex core in Fig. 10(b) becomes an ellipse.

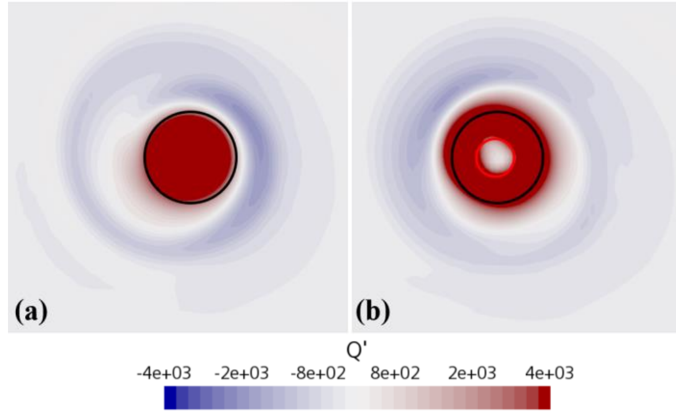

Fig. 10 Q' cloud comparison between wetted and cavitation condition.

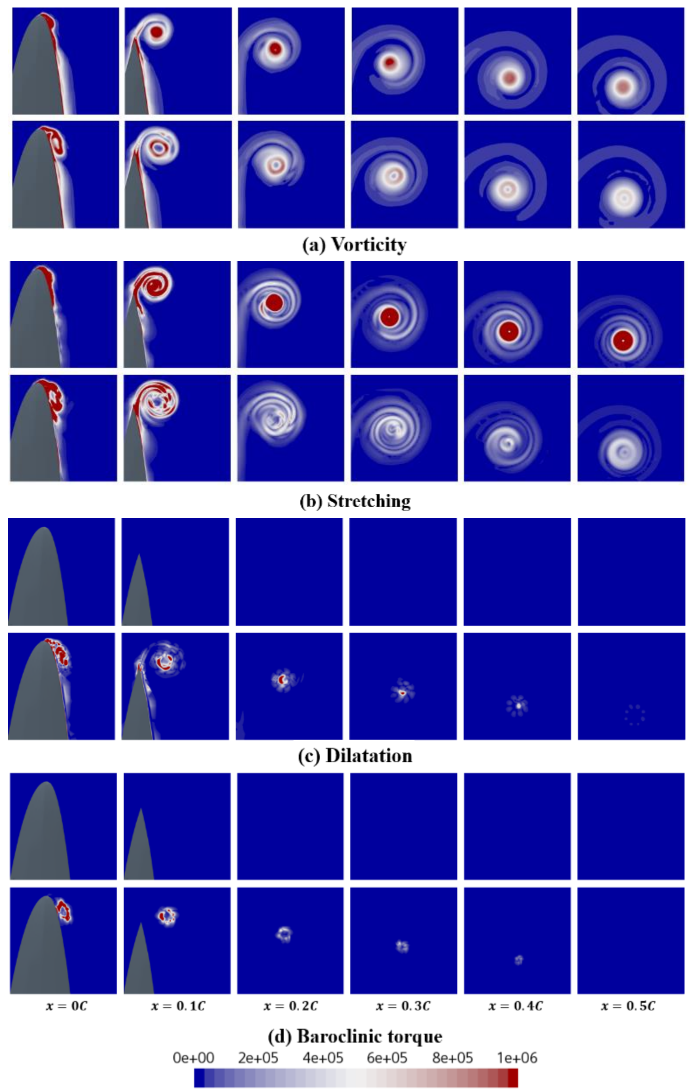

Fig. 11 Contours of the terms of the vorticity transport equation, in the upper column for wetted flow and in the lower column for cavitating flow.

Furthermore, to quantify the interaction between cavitation and tip vortex, based on the vorticity transport equation, the effects of cavitation on each component of vortex has been calculated and visualized. The vorticity transport equation is as follows:

$$\frac{D\omega}{Dt}=(\omega\cdot\nabla)V-\omega(\nabla\cdot V)+\frac{\nabla\rho_m\times\nabla p}{\rho_m^2}+\frac{1}{Re}(\nabla^2\omega) \tag{26}$$

Where the terms on the right hand represent the stretching, dilatation, baroclinic torque, and viscosity term, respectively. Among them, since the viscosity term is very small and can be negligible, it is not discussed in here. The rest are shown in Fig. 11: upper column for wetted flow condition and the lower for cavitation flow.

When comparing the vorticity distribution between different position in Fig. 11(a), it can be shown that as the tip vortex develops backward, the tip vortex appears to diffusion phenomenon, that is, the tip vortex area gradually increases but the vortex core gradually shrinks (from x=0C to x=0.5C).

And in the next step, after the comparison for different conditions, we find that in wetted flow condition, due to the incompressibility of the fluid, the dilatation term and baroclinic torque term are zero, as expected with the theory. And for wetted flow, there is apparent swirling motion in the tip vortex core, but when cavitation occurs, a non-swirl zone will be formed in the center of the vortex core, as shown in Fig. 11(a). In the wetted flow, the stretching term is absolutely dominating, and the other terms are basically zero. In the cavitation flow, the stretching distribution around vortex core area in the wetted flow is smeared by cavitation in Fig. 11(b). The cavitation bubble hugely weakened vortex stretching effect. Simultaneously, after the generation of cavitation, the tip vortex dilatation term and baroclinic torque term mainly occurs at the interface of the vapor and water, which is zero in wetted flow. That is, the density gradient and mass exchange caused by cavitation at this location influent the vortex transport process, just as illustrated in Fig .11(c) and (d).

TVC Control

In order to inhibit the harmful effects caused by tip vortex cavitation and control the development of TVC, this paper open seven 0.5mm-dimater holes on the hydrofoil surface injecting water to suppress TVC. By this method, the effect of water injection on the development of cavitation has been studied. According to the experiment by Lee *et al*. (2018), the injection holes are selected on the tip and within the inception region of tip vortex cavitation. The locations of injection holes are illustrated in Fig. 12, and their coordinates are shown in Table 3.

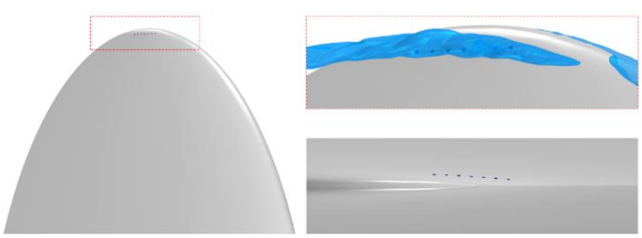

Fig. 12 The locations of injection holes on hydrofoil surface

Along the normal direction of the holes, water was injected into cavitation region and the injection speed $V_J = 1.5V_I$. The comparison result is visualized by volume fraction isosurface of water vapor $\alpha_v = 0.1$ in Fig. 13. It is clearly shown that the injection affects cavitation development enormously. With the impact of water injection, the vapor volume decreases to $3.0\times10^{-7}m^3$ from $3.8\times10^{-7}m^3$. And attenuation rate is about 26.7%.

Table 3. The coordinates of injection holes.

Item	X Position (m)	Z Position (m)
Hole 1	0.0730	0.174
Hole 2	0.0745	0.174
Hole 3	0.0760	0.174
Hole 4	0.0775	0.174
Hole 5	0.0790	0.174
Hole 6	0.0805	0.174
Hole 7	0.0820	0.174

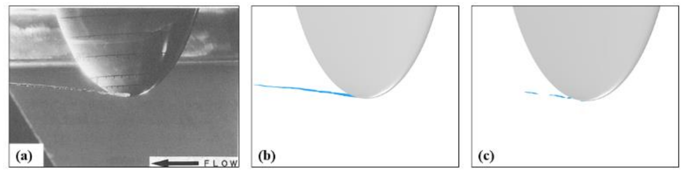

Fig. 13 Comparison of TVC between cavitation condition and water injection condition: (a) experiment result by Nobuhide Takasugi (1992); (b) $\alpha_v = 0.1$ in cavitation flow; (c) $\alpha_v = 0.1$ in water injection condition

In the next step, to analyze the mechanism of injection effects to cavitation, the flow around injection holes have been illustrated in Fig. 14. And Q-criterion cloud also be involved in this figure to find out the influence of water injection to tip vortex. According to the Fig. 14(a)~(g) on the left column, the flow around tip region can be divided into two parts. Firstly, the fluid on the pressure side has the upward movement towards to tip position. When the fluid moves upward over the tip region to the suction side, the upward movement trend gradually disappeard and began to move downward. Secondly, just like the flow trend shown in Fig. 7(b), the flow on the suction side is not simply to the root of the hydrofoil. Near the tip position, the suction side flow has the trends to the tip region. In Fig. 14 in left colume, this phenomenon appears as re-entrant flow near the wall on the suction side. These two parts of flow lead to the generation of tip vortex and TVC.

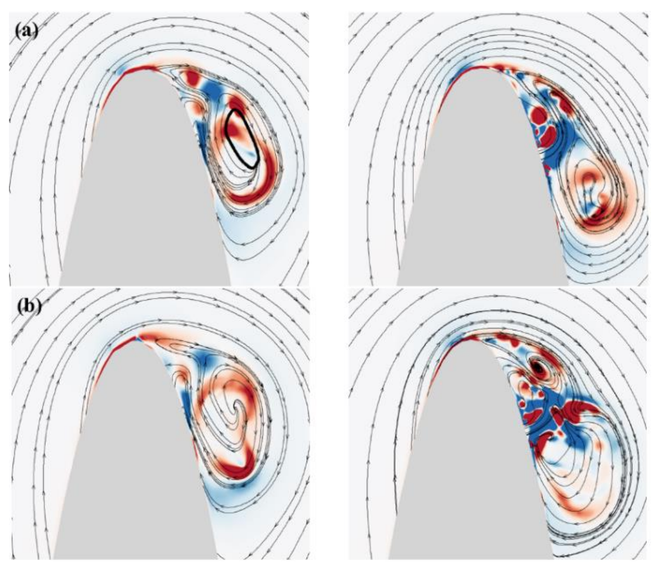

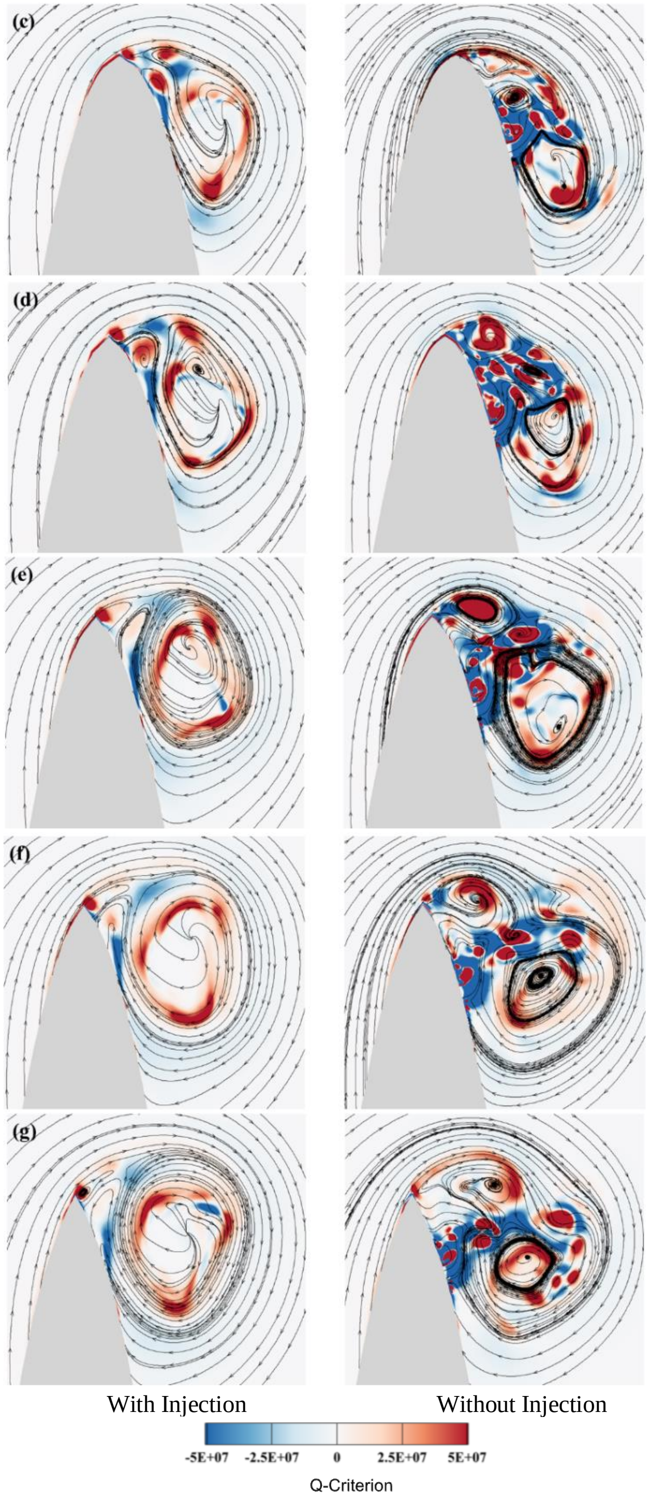

Fig. 14 Flow trend comparison between cavitation and injection condition: (a)~(g) represent hole 1~7.

When injecting water at the tip region, the injection hindered the re-entrant flow near the wall, which affected the structure of tip vortex and inhibited the generation of cavitation. At the same time, when comparing the cloud in right column in Fig. 14, it is clearly shown that the flow around the tip vortex region of the hydrofoil also have effects to the injection flow. After the injection from holes, part of the injection flow formed vortex below the positions of the hole along with the re-entrant flow. and the other part moved upward to form vortex, which has an opposite rotation direction with the vortex around the region below to injection holes. This phenomenon is particularly obvious in Fig. 14(b)~(f).

CONCLUSION

Based on the IDDES turbulence model and the Schnerr-Sauer cavitation model, this paper uses adaptive meshing refinement methods to capture the tip vortices cavitation phenomenon of NACA0012 elliptical hydrofoil. Firstly, this paper mainly visualized the flow around the surface of hydrofoil, analyzed the mechanism of the generation of tip vortex and its cavitation and secondly used mass injection method to control tip vortex cavitation, the result shows that water injection can effectively suppress TVC development.

a) According to the flow field analysis, the flow around hydrofoil shows the characteristic of rotating from the pressure to suction side. With this trend and the effect of the re-entrant flow near the suction surface of the tip, tip vortex is produced.

b) Swirling effect of the tip vortex reduced the pressure distribution in the vortex core zone and leaded to generating of TVC. At the same time, cavitation also affected tip vortex. On the one hand, it increased the diameter of the vortex core region and slightly changed the structure of the tip vortex core; on the other hand, it has a huge influence to the vortex transporting process: weakened vortex stretching effect and enlarged the dilatation and baroclinic torque terms.

c) By water injection, TVC can be successful controlled. The injection act on the inhibition of development of the tip vortex cavitation through affecting the re-entrant flow near the hydrofoil surface.

d) In the next research, the influence of water injecting angle and velocity to tip vortex cavitation will be analyzed.

ACKNOWLEDGEMENTS

This work is supported by National Natural Science Foundation of China (52001210, 51879159, 52131102), the Oceanic Interdisciplinary Program of Shanghai Jiao Tong University (SL2020PT104), to which the authors are most grateful.

REFERENCES

Cao, L. S., Huang, F. L., Liu, C., Wan, D. C. (2021). Vortical structures and wakes of a sphere in homogeneous and density stratified fluid. Journal of Hydrodynamics. 33(2): 207-215.

Chang, N., Ganesh, H., Yakushiji, R., & Ceccio, S. L. (2011). Tip vortex cavitation suppression by active mass injection. Journal of Fluids Engineering, 133(11).

Chen, K. J. (2019). Numerical Simulation of cavitation around hydrofoil and propeller based on OpenFOAM. SJTU.

Chen, G., Li, X. B., & Liang, X. F. (2022). IDDES simulation of the performance and wake dynamics of the wind turbines under different turbulent inflow conditions. Energy, 238.

Cheng, H. Y., Bai, X. R., Long, X. P., Ji, B., Peng, X. X., & Farhat, M. (2020). Large eddy simulation of the tip-leakage cavitating flow with an insight on how cavitation influences vorticity and turbulence. Applied Mathematical Modelling, 77, 788-809.

Gritskevich, M. S., Garbaruk, A. V., Schütze, J., Menter, F. R. (2011). Development of DDES and IDDES Formulations for the k-ω Shear Stress Transport Model. Flow, Turbulence and Combustion, 88(3), 431-449.

Ji, B., Luo, X., Arndt, R. E., & Wu, Y. (2014). Numerical simulation of three dimensional cavitation shedding dynamics with special emphasis on cavitation–vortex interaction. Ocean Engineering, 87, 64-77.

Lee, C. S., Ahn, B. K., Han, J. M., & Kim, J. H. (2018). Propeller tip vortex cavitation control and induced noise suppression by water injection. Journal of marine science and technology, 23(3), 453-463.

Liu, F. X. (2019). Numerical simulation and noise analysis of propeller tip vortex cavitation. SJTU.

Naz, Y., Mehmet, A., and Mahdi, K. (2019). "An improved Mesh Adaption and Refinement approach to Cavitation Simulation (MARCS) of propellers". Ocean Engineering,171, 139-150.

Ohta, T., & Sugiura, R. (2019). Numerical prediction of interaction between turbulence structures and vortex cavitation. Journal of Turbulence, 20(10), 599-625.

Takasugi, N., Yamaguchi, H., Kato, H., Maeda, M. (1992). An experiment of cavitating flow around a finite span hydrofoil. Journal of the Society of Naval Architects of Japan. 1992(172), 257-265.

Timoshevskiy, M. V., & Zapryagaev, I. I. (2017). Generation of a wall jet to control unsteady cavitation over a 2D hydrofoil: visualization and hydroacoustic signal analysis. In Journal of Physics: Conference Series (Vol. 899, No. 3, p. 032021). IOP Publishing.

Wang, J., Minelli, G., Dong, T., Chen, G., & Krajnović, S. (2019). The effect of bogie fairings on the slipstream and wake flow of a high-speed train. An IDDES study. Journal of Wind Engineering and Industrial Aerodynamics, 191, 183-202.

Xie, CM., Liu, JY., Jiang, JW., Huang, WX. (2021). Numerical study on wetted and cavitating tip-vortical flows around an elliptical hydrofoil: Interplay of cavitation, vortices, and turbulence. Physics of Fluids, 33(11), 112108.